
REDUCING ALEATORIC AND EPISTEMIC UNCERTAINTY THROUGH MULTI-MODAL DATA ACQUISITION

Arthur Hoarau

CNRS, Université de technologie de Compiègne
UMR CNRS 7253 Heudiasyc, France
arthur.hoarau@utc.fr

Benjamin Quost

Université de technologie de Compiègne
UMR CNRS 7253 Heudiasyc, France
benjamin.quost@utc.fr

Sébastien Destercke

CNRS, Université de technologie de Compiègne
UMR CNRS 7253 Heudiasyc, France
sebastien.destercke@utc.fr

Willem Waegeman

University of Ghent
Ghent, Belgium
willem.waegeman@UGent.be

ABSTRACT

To generate accurate and reliable predictions, modern AI systems need to combine data from multiple modalities, such as text, images, audio, spreadsheets, and time series. Multi-modal data introduces new opportunities and challenges for disentangling uncertainty: it is commonly assumed in the machine learning community that epistemic uncertainty can be reduced by collecting more data, while aleatoric uncertainty is irreducible. However, this assumption is challenged in modern AI systems when information is obtained from different modalities. This paper introduces an innovative data acquisition framework where uncertainty disentanglement leads to actionable decisions, allowing sampling in two directions: sample size and data modality. The main hypothesis is that aleatoric uncertainty decreases as the number of modalities increases, while epistemic uncertainty decreases by collecting more observations. We provide proof-of-concept implementations on two multi-modal datasets to showcase our data acquisition framework, which combines ideas from active learning, active feature acquisition and uncertainty quantification.

1 Introduction

Machine learning models are increasingly used to make decisions affecting people’s lives, such as in medical diagnosis, law enforcement, police investigation, insurance and loan approval, or environmental permit deliverance. Because incorrect decisions can have significant consequences, these systems must not only be accurate, but also provide a credible measure of their own uncertainty, warranting whenever model outputs should be trusted. Therefore, the problem of uncertainty quantification is currently the focus of many research works, a number of which are dedicated to distinguish between two specific types of uncertainty, known as aleatoric and epistemic (Hora, 1996; Kendall & Gal, 2017; Hüllermeier & Waegeman, 2021; Bengs et al., 2023; Lakshminarayanan, 2024).

Aleatoric uncertainty is due to inherent randomness, and is generally assumed to be irreducible. Epistemic uncertainty arises from a lack of knowledge about the true data-generating distribution, and can be reduced by collecting more data. Typically, a machine learning model uses an estimate of the (unknown) true probability distribution of the data based on a training set. Epistemic uncertainty reflects the difference between this estimate and the actual distribution, and methods estimating this type of uncertainty usually construct a (second-order) distribution over probability vectors (see Section 2 for more details).

To generate accurate and reliable predictions, modern AI systems often need to combine data from multiple modalities, such as text, images, audio, spreadsheets, and time series. This requirement has led to the emergence of a research field known as multi-modal machine learning (Baltrusaitis et al., 2018; Liang et al., 2024), introducing new opportunities and challenges for disentangling uncertainty. More specifically, the irreducibility assumption of aleatoric uncertainty can be challenged when information is obtained from different modalities. Future-proof general AI systems should be able to “search for evidence” to make complex decisions with high reliability. For example, in medical diagnostics,

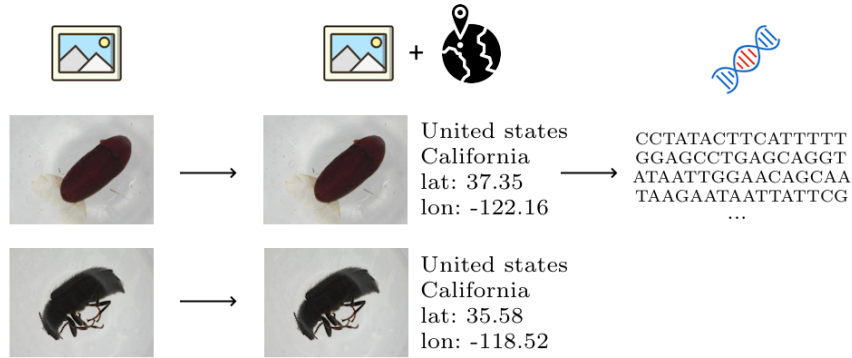


Figure 1: Active learning with multi-modal feature acquisition illustrated on two test instances from the BIOSCAN-5M dataset. For the first insect, all three modalities are needed to decrease the aleatoric uncertainty to a satisfactory level, whereas for the second insect, one is sufficient certain after adding geographical information to the image modality.

an AI assistant for patient examination could begin with simple procedures, such as blood or urine tests, and potentially follow up with more complicated (and expensive) investigations, such as MRI, CT, or genetics-based scans that uncover additional modalities. One then expects the aleatoric uncertainty about the diagnosis to decrease as more informative (yet more expensive) modalities are queried (Acosta et al., 2022). Similar AI assistants can also be useful in other application domains, such as police investigations, customs checks, and failure monitoring in industrial processes.

Motivated by potential use cases in such domains, this paper introduces a novel data acquisition framework for multi-modal data by disentangling aleatoric and epistemic uncertainties, which we believe is crucial for multi-modal sampling problems. This original approach involves reducing both types of uncertainties through querying additional instances and modalities, which will be realized with a two-stage backtracking protocol that “searches for evidence”. Several data acquisition approaches, such as active learning (Settles, 2009) and active feature acquisition (Li & Oliva, 2020), have demonstrated that iteratively gathering more knowledge can enhance performance in machine learning. However, knowledge acquisition (whether through new observations or additional modalities) can be costly, making an effective data collection strategy essential.

Our new protocol combines active learning and active feature acquisition for multi-modal sampling. On a high level, this protocol proceeds as follows. Step 1: Assess epistemic uncertainty for a new test instance with an initial set of modalities: if epistemic uncertainty is high, collect more labelled training instances that are similar to the test instance, while measuring the same modalities. Step 2: Once epistemic uncertainty has been reduced, check aleatoric uncertainty: if it is high, sample an additional modality and return to Step 1. If it is low, proceed to Step 3: Make a prediction for the test instance as soon as epistemic and aleatoric uncertainty are both sufficiently low.

As a practical illustration, let’s consider the the BIOSCAN-5 dataset, which is an insect classification task that will be more thoroughly explained in the experimental section. The dataset has three modalities that can be queried to obtain reliable predictions: images, geographical information and DNA sequences. The protocol is illustrated for two insects in Figure 1. For the first one DNA had to be sequenced before a prediction with sufficient certainty could be generated, whereas for the second observation it sufficed to analyze the image and the geographical information.

The paper is structured as follows. Section 2 presents related work on uncertainty disentanglement, active learning and active feature acquisition. Section 3 formalizes the proposed protocol of active learning with multi-modal feature acquisition, together with different methods to quantify both epistemic and aleatoric uncertainties. Section 4 presents two experiments, first on a simple dataset to illustrate the behavior of the method, then on the above-mentioned BIOSCAN-5 dataset with multiple modalities. Our experimental results also shed new light on uncertainty disentanglement, and the properties that a proper epistemic uncertainty metric should satisfy. Finally, Section 5 concludes the article. To simplify reproducibility, we make our framework available to the scientific community: <https://github.com/ArthurHoa/deep-eknn>. It is compatible with pre-trained models and can be seamlessly integrated at the penultimate layer of a neural network.

2 Background and related work

Uncertainty disentanglement. To disentangle aleatoric and epistemic uncertainty, numerous methods have been proposed in recent years (Huang et al., 2024). Such methods can be grouped into different families of models, but most of these families leverage the training phase to estimate a distribution of probabilities (as opposed to a single point estimate).

Bayesian methods compute a posterior distribution over the parameters of an ML model and construct a second-order distribution over class probabilities via Bayesian model averaging (Kendall & Gal, 2017; Depeweg et al., 2018). Conversely, evidential deep learning takes a frequentist statistics perspective and introduces specific loss functions to estimate a parametric second-order distribution over class distribution, without the need for specifying a prior and posterior over the parameters. For multi-class classification problems typically the Dirichlet distribution is chosen as second-order distribution (Sensoy et al., 2018; Malinin & Gales, 2018; 2019; Ulmer et al., 2023). Ensemble methods represent epistemic uncertainty via ensemble diversity, which can be realized by randomizing the training data via bootstrapping, randomizing a neural network architecture via techniques such as MC Dropout, or randomizing the optimizer as in Deep Ensembles (Lakshminarayanan et al., 2017; Nguyen et al., 2023; Mobiny et al., 2021; Shaker & Hüllermeier, 2020). Some of these methods have been interpreted as obtaining a sample of the second-order distribution (Gal, 2016). Density-based and distance-based methods usually model aleatoric and epistemic uncertainty in a direct way (Nguyen et al., 2022; Hoarau et al., 2024; Van Amersfoort et al., 2020; Sun et al., 2022; Liu et al., 2020), but these methods can also construct the second-order distribution in a post-processing step (Charpentier et al., 2020; 2022). All methods can disentangle and measure both aleatoric and epistemic uncertainty using metrics like entropy, variance, or pseudo-counts (Wimmer et al., 2023; Schweighofer et al., 2023; Sale et al., 2023; Duan et al., 2024).

Active learning. Given the cost of collecting labels in classification, a trade-off between performance and labeling cost has been proposed. Active learning (AL) (Settles, 2009) aims to select the most relevant observations to be labeled, thereby reducing the number of labeled data points and the associated costs (Hacohen et al., 2022). The most common approach is pool-based sampling, where classes of unlabeled observations (referred to as *instances* in AL) are queried one by one or in batches. Various methods have been proposed, such as random sampling, where labels are queried randomly as the labeled dataset grows. The method most relevant to our paper is uncertainty sampling (Lewis & Gale, 1994), where the learner tries to reduce its uncertainty by querying the labels for which it would be the least certain. More specifically linked to our work, epistemic uncertainty sampling, focusing on the reducible areas of uncertainty, has been implemented using various techniques such as density-based methods (Nguyen et al., 2022; Hoarau et al., 2024) or Bayesian approaches (Houlsby et al., 2011; Shelmanov et al., 2021).

Active feature acquisition. Active learning focuses on selecting which observations and labels to query, while active feature acquisition concentrates on the variables. Many problems are characterized by missing variables, and feature acquisition (FA) offers potential solutions for addressing variable collection, the goal being to collect the most informative variables during training to improve the model (Zheng & Padmanabhan, 2002). This should be distinguished from feature collection at test stage, whose purpose is to minimize misclassification costs (or a variant thereof) during the test phase (Greiner et al., 2002; Quost, 2021). Recently, several methods for active feature acquisition have been applied to deep architectures and multi-modal data (Li & Oliva, 2020; Shim et al., 2018; Kossen et al., 2023). While active learning focuses on observations and feature acquisition on variables, our approach leverages a proper modeling of uncertainty at both training and prediction time to improve reliability, by focusing on both observations and variables with different modalities.

3 Active learning with multi-modal feature acquisition

The proposed Active Learning with multi-modal Feature Acquisition (ALFA) strategy minimizes predictive uncertainty, while keeping associated costs in check. We first introduce our active learning with multi-modal feature acquisition strategy proposal in Section 3.1, and then present the four methods employed to quantify epistemic and aleatoric uncertainties in our study in Section 3.2.

3.1 Formal description of the algorithm

Let us first describe the inference algorithm on a high level. Given a new test observation, the model’s EU (Epistemic Uncertainty) is calculated, reflecting its level of knowledge about a given problem. If this uncertainty is too high (indicating a lack of knowledge), new observations similar to the one being processed are added to the training set to reduce the model’s ignorance. Once the EU is sufficiently low, the model’s AU (Aleatoric Uncertainty) can be assessed, representing the inherent difficulty of predicting the class given the current variables. If the AU is too high,

Algorithm 1 Active learning with feature acquisition**Require:** $t_e, t_a, \mathbf{x}, \mathcal{D}_{\mathcal{L}}^j, \mathcal{D}_{\mathcal{U}}^j$ **Ensure:** $t_e, t_a \in \mathbb{R}$ $j \leftarrow 1$

▷ Initial (simple) representation space

train model on $\mathcal{D}_{\mathcal{L}}^j$ **do** compute $EU^j(\mathbf{x})$ **while** $EU^j(\mathbf{x}) \geq t_e$ **do** $x_{\text{new}} \leftarrow \text{Query_strategy}(\mathbf{x}, \mathcal{D}_{\mathcal{U}}^j)$ label $\leftarrow \text{Query_label}(x_{\text{new}})$ $\mathcal{D}_{\mathcal{U}}^j.\text{Remove}(x_{\text{new}})$ $\mathcal{D}_{\mathcal{L}}^j.\text{Append}((x_{\text{new}}, \text{label}))$ train model on $\mathcal{D}_{\mathcal{L}}^j$ compute $EU^j(\mathbf{x})$ **end while** compute $AU^j(\mathbf{x})$ **if** $AU^j(\mathbf{x}) \geq t_a$ **then** $j \leftarrow j + 1$

▷ Retrieve additional modality

 train model on $\mathcal{D}_{\mathcal{L}}^j$ **end if****while** $AU^j(\mathbf{x}) \geq t_a$ make prediction on \mathbf{x}

▷ Reliable prediction

since no additional knowledge can reduce it, a new representation space is created by acquiring new modalities. When both EU and AU are judged sufficiently low, the model is deemed to possess sufficient knowledge and descriptors to make a reliable prediction for the given instance. At this point, the process stops.

More formally, we consider a sequence of μ input spaces $\mathcal{I} = (\mathcal{X}^1, \dots, \mathcal{X}^\mu)$ associated with the same output space $\mathcal{Y} = \{y_1, \dots, y_K\}$, with $K \geq 2$. For each input space we assume $\mathcal{X}^j = \mathbb{R}^{P_j}$, with $j \leq \mu$, \mathcal{X}^j being a collection of P_j random variables from different modalities. We denote by \mathbf{x}^j an instance in space \mathcal{X}^j , and by (\mathbf{x}_i^j, y_i) a labeled training instance sampled *i.i.d* from the unknown probability measure \mathcal{P}^j .

We assume that the collection \mathcal{I} has a fixed order and is uncovered iteratively via Algorithm 1, starting from \mathcal{X}^1 and stopping at \mathcal{X}^μ when the algorithm ends. We assume that modalities are ordered by acquisition cost, with a higher cost being compensated by the decisiveness of the underlying information. Figure 1 depicts a practical scenario where images are collected first, followed by geographical information, and DNA is sequenced only if really necessary. Remark that this setup is different from some papers on active feature acquisition, which assume that the sequence of classifiers varies over test instances (Clertant et al., 2019).

Training phase. We first describe the training phase, before predictions are made for test instances. Given μ hypothesis spaces \mathcal{H}^j , $j \leq \mu$, composed of hypotheses $h^j : \mathcal{X}^j \rightarrow \mathcal{Y}$ mapping any instance \mathbf{x}^j to an outcome y , we train models \hat{h}^j based on a labeled training set $\mathcal{D}_{\mathcal{L}}^j = \{(\mathbf{x}_i^j, y_i) | i \in \Phi_{\mathcal{L}}^j\}$, for all $j \leq \mu$ (the indices $i \in \Phi_{\mathcal{L}}^j$ point out to the labeled instances). For active learning purposes, we assume that we also have access to an unlabeled training set $\mathcal{D}_{\mathcal{U}}^j = \{\mathbf{x}_i^j | i \in \Phi_{\mathcal{U}}^j\}$ with instances defined in the same space \mathcal{X}^j .

Inference phase. We are now ready to sketch our active learning with multi-modal feature acquisition strategy, detailed in Algorithm 1. When one needs to predict the class of a new incoming instance \mathbf{x} , the first input space (generally composed of the cheapest variables or modalities, *i.e.* the easiest to acquire) is queried such that the instance space of the new incoming instance $\mathcal{X}_{\mathbf{x}}$ is compatible with h^1 , $\mathcal{X}^1 \subseteq \mathcal{X}_{\mathbf{x}}$. A prediction $\hat{y} = \hat{h}^1(\mathbf{x})$ can thus be made.

Unlike the classical classification setting, this decision is in our procedure not necessarily final. If the EU is above a certain threshold (*i.e.*, $EU^1(\mathbf{x}) \geq t_e$), a new observation from the unlabeled set $\mathcal{D}_{\mathcal{U}}^1$ is added to the labeled set $\mathcal{D}_{\mathcal{L}}^1$ with its true class in \mathcal{Y} . Observations can be added one by one, or by batches — the latter is called pool-based sampling in active learning (Settles, 2009).

Otherwise, if the EU is acceptable (*i.e.*, $EU^1(\mathbf{x}) < t_e$), the AU is computed. If the latter is above a certain threshold (*i.e.*, $AU^1(\mathbf{x}) \geq t_a$), new modalities are added to $\mathcal{X}_{\mathbf{x}}$ such that the instance space of the new incoming instance $\mathcal{X}_{\mathbf{x}}$ is

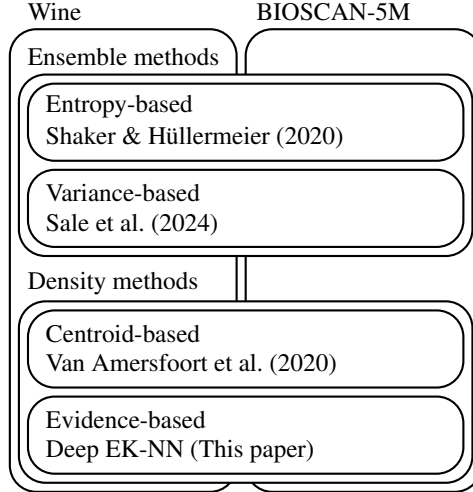


Figure 2: Experiments on Wine and BIOSCAN-5M with uncertainty estimation through four different methods.

compatible with h^2 , $\mathcal{X}^2 \subseteq \mathcal{X}_x$. These two steps are repeated with EU^2 and AU^2 and the process continues with EU^j and AU^j , for $j \leq \mu$. Whenever the AU for any model \hat{h}^j is below the threshold (*i.e.* $\exists j \leq \mu$, $AU^j(\mathbf{x}) < t_a$), then the state of knowledge is deemed sufficient for a decision to be safely made, and the process is stopped.

3.2 Uncertainty disentanglement

Our study investigates four state-of-the-art approaches to disentangle aleatoric and epistemic uncertainty. Among the four main families of approaches discussed in Section 2, we focus on ensemble and density-based methods. Ensemble methods have been interpreted as Bayesian estimators by generating samples from the posterior second-order distribution (Mobiny et al., 2021; Shaker & Hüllermeier, 2020), so our study also incorporates Bayesian methods in an implicit way. We do not consider evidential deep learning methods, because these methods have faced increasing criticism (Meinert et al., 2022; Bengs et al., 2023; Jürgens et al., 2024) regarding EU estimation (*cf.*, Appendix C). We also consider various metrics to quantify aleatoric and epistemic uncertainty.

For entropy-based uncertainty estimation, we used the entropy decomposition method described in (Shaker & Hüllermeier, 2020). Here, the posterior distribution is approximated by a finite ensemble of estimators. The AU can be obtained as follows:

$$AU(\mathbf{x}) = -\frac{1}{M} \sum_{i=1}^M \sum_{y \in \mathcal{Y}} p(y|h_i, \mathbf{x}) \log_2 p(y|h_i, \mathbf{x}), \quad (1)$$

with M the number of estimators. Total Uncertainty (TU) can be approximated in terms of Shannon’s entropy of the predictive posterior distribution as follows:

$$TU(\mathbf{x}) = -\sum_{y \in \mathcal{Y}} \left(\frac{1}{M} \sum_{i=1}^M p(y|h_i, \mathbf{x}) \right) \times \log_2 \left(\frac{1}{M} \sum_{i=1}^M p(y|h_i, \mathbf{x}) \right). \quad (2)$$

Finally, EU can be derived through additive decomposition as $EU(\mathbf{x}) = TU(\mathbf{x}) - AU(\mathbf{x})$.

For variance-based uncertainty estimation, we investigated the label-wise variance decomposition approach proposed in (Sale et al., 2024). TU is defined for each class as the variance of the outcomes, and global uncertainty is obtained by summing over all classes as follows:

$$TU(\mathbf{x}) = \sum_{y \in \mathcal{Y}} \text{Var}(Y_y), \quad (3)$$

where Y_y are binary outcomes according to a K -dimensional random vector indicating the presence or absence of a particular label $y \in \mathcal{Y}$. AU is defined as the expected conditional variance, as follows:

$$AU(\mathbf{x}) = \sum_{y \in \mathcal{Y}} \mathbb{E} [\Theta_y(1 - \Theta_y)], \quad (4)$$

with $\Theta_y = P(Y_y = 1)$ associated to a random vector distributed according to a second-order distribution; whereas EU corresponds to the expected reduction in squared-error loss, defined as follows:

$$EU(\mathbf{x}) = \sum_{y \in \mathcal{Y}} \text{Var}(\Theta_y). \quad (5)$$

For density-based methods, we examined the centroid-based approach presented in (Van Amersfoort et al., 2020). To compute the model’s uncertainty, the authors proposed measuring the distance from the incoming observation to the class centroids using a radial basis function:

$$U_y(\mathbf{x}, \mathbf{e}_y) = \exp \left[-\frac{\frac{1}{n} \|\mathbf{W}_y \hat{h}(\mathbf{x}) - \mathbf{e}_y\|_2^2}{2\sigma^2} \right], \quad (6)$$

with \hat{h} the model, \mathbf{e}_y the centroid associated with class y and \mathbf{W}_y a weight matrix of size n (centroid size) by d (feature extractor output size) in the case of a deep architecture. The length scale σ is an hyper-parameter of the method. The epistemic certainty \mathcal{C} associated with instance \mathbf{x} is then obtained by measuring the distance from the incoming observation to the nearest class centroid:

$$\mathcal{C}(\mathbf{x}) = \max_{y \in \mathcal{Y}} U_y(\mathbf{x}, \mathbf{e}_y), \quad (7)$$

while AU is computed based on the relative distances between all clusters. Deep EK-NN, the second density-based method, computes EU and AU based on the nearest neighbors of the incoming test instance. The procedure is detailed in Appendix A.

These four methods were implemented and used within the proposed ALFA framework on two different datasets, as illustrated in Figure 2.

4 Experiments

In this section, we present the results obtained using our proposal for Active Learning with multi-modal Feature Acquisition (ALFA) in two scenarios. Since very few experimental multi-modal datasets with associated costs for modalities are available in the public domain, we first use the Wine dataset from the UCI repository (Dua & Graff, 2017) to illustrate the concept; and we then apply our proposal to a real-world deep learning case involving multiple modalities, including tabular data, images, and DNA sequences. In the experiments, we employ the four uncertainty quantification methods described in Section 3.2, according to Figure 2.

4.1 Application to Wine dataset

This section describes the behavior of the proposed ALFA method on a simple dataset before its practical application to a multi-modal dataset. The tabular dataset consists of variables grouped according to an assigned fictitious cost. The four groups are an ignition study, a visual study, a chemical study, and an acidity study. Further details about this experiment are provided in Appendix D.

ALFA provides a protocol for assessing the reliability of a given prediction. If the EU is too high, additional labels must be queried; if the AU is too high, new variables must be added. To obtain a comprehensive understanding of the method’s behavior, a model is trained on four variable spaces (with increasing querying costs) and with varying sample sizes (with increasing labeling costs) for each variable space.

Regarding uncertainty quantification, density-based Deep EK-NN is initially trained on the variables derived from the ignition study. Its performance, shown in Figure 3a, improves as the training set size increases. This process is repeated until all variables are included in the dataset, as depicted in Figure 3d, incorporating variables from the ignition, visual, chemical, and acidity studies. Two expected behaviors are observed: on one hand, more labeled observations lead to better performance, and on the other hand, adding more variables also improves performance.

At any given stage of the learning process, ALFA provides reliable predictions as well as an acquisition protocol for non-reliable ones. Figures 3e to 3h display the number of reliable predictions alongside the model’s performance on this reliable subset. As expected, the model’s performance on the reliable subset is significantly higher than its overall performance at every learning stage. Intuitively, the number of reliable predictions increases with the inclusion of more variables (a more expensive model), ranging from 10-15 in Figure 3e to 45-52 in Figure 3h, out of 54 test instances.

This study was also conducted for various state-of-the-art methods for quantifying uncertainty. Two ensemble methods (entropy-based and variance-based) and two density-based methods (centroid-based and Deep EK-NN) were analyzed,

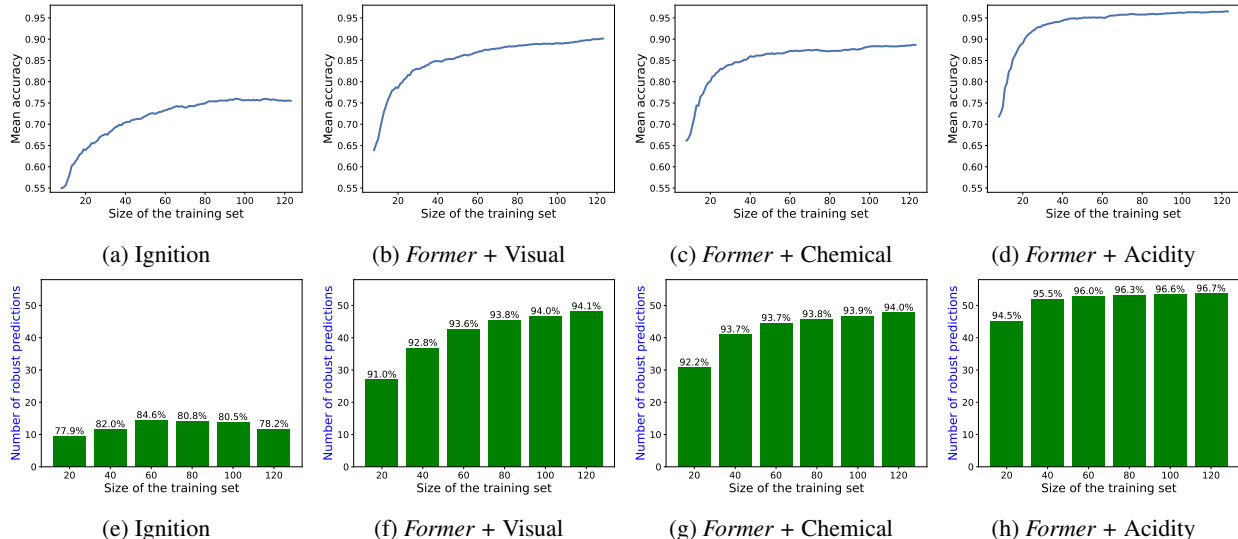


Figure 3: Global test performance (top) and number of robust predictions with test performance for robust predictions (bottom) for each model vs. size of the training set on Wine dataset with Deep EK-NN.

as outlined in Section 3.2. Ensemble-based and density-based methods respectively exhibit similar behavior regarding ALFA.

All four methods performed as expected within the proposed ALFA strategy. Ensemble-based methods are slightly less effective at quantifying uncertainty in the context of ALFA, although they achieve better peak raw performance on fully labeled datasets. This advantage can be attributed to the use of random forests, which face fewer limitations compared to density-based methods.

These latter, however, appear to be better suited for quantifying uncertainty in the ALFA framework. The centroid-based method and Deep EK-NN demonstrate comparable performance in terms of reliable predictions, with a nearly identical number of reliable predictions.

4.2 Application to BIOSCAN-5M

We applied our ALFA approach to the multi-modal BIOSCAN-5M (Gharaee et al., 2024) dataset, which includes images (photos), geographical information, and DNA sequences of various insects. This dataset is described in more detail in Appendix E. We recall the objective of the method, which is to provide reliable predictions or offer a cost-effective resolution protocol when these predictions are not reliable.

Three models, each associated with a querying cost, are trained independently: a model based solely on the image of the insect (with a low acquisition cost), a model using images enriched with geographical data (with a higher yet reasonable cost), and a model based on the individual’s DNA sequence (high cost as it requires sequencing the insect’s DNA). Naturally, the model leveraging DNA sequences is the most accurate, followed by the one using images enriched with geographical data, and finally the one using images only. We get back to the example highlighted in the introduction in Figure 1. It presents ALFA applied to two insects of the order *Coleoptera*. Both test instances are analyzed in light of their respective ALFA process.

The picture of the first *Coleoptera* is initially queried as it represents the least costly form of observation. Starting from this point, the first model (trained on a limited number of observations, specifically 1000 in a 10-class classification setup, as detailed in Appendix E) attempts to predict the corresponding class. As long as EU remains above the threshold ($EU \geq t_e$), reflecting the model’s lack of knowledge, active learning is considered to add new observations to the dataset to reduce it. Once the model achieves sufficient confidence (in this case with 17000 images in the training set, which represents a 66% reduction in labeling cost compared to a full training set of 50000 labels), the AU of the model is computed. If AU falls below the threshold t_a , the problem is considered sufficiently simple for a prediction to be made. However, in our practical scenario, we found that $AU \geq t_a$, indicating that the classification problem remained too complex based on images only. At this stage, a more expressive (and typically more expensive) representation space must be used, and the model was therefore enriched with geographical information. In this case, 14000 observations (image + geographical information) were required to reduce EU down to the threshold; yet,

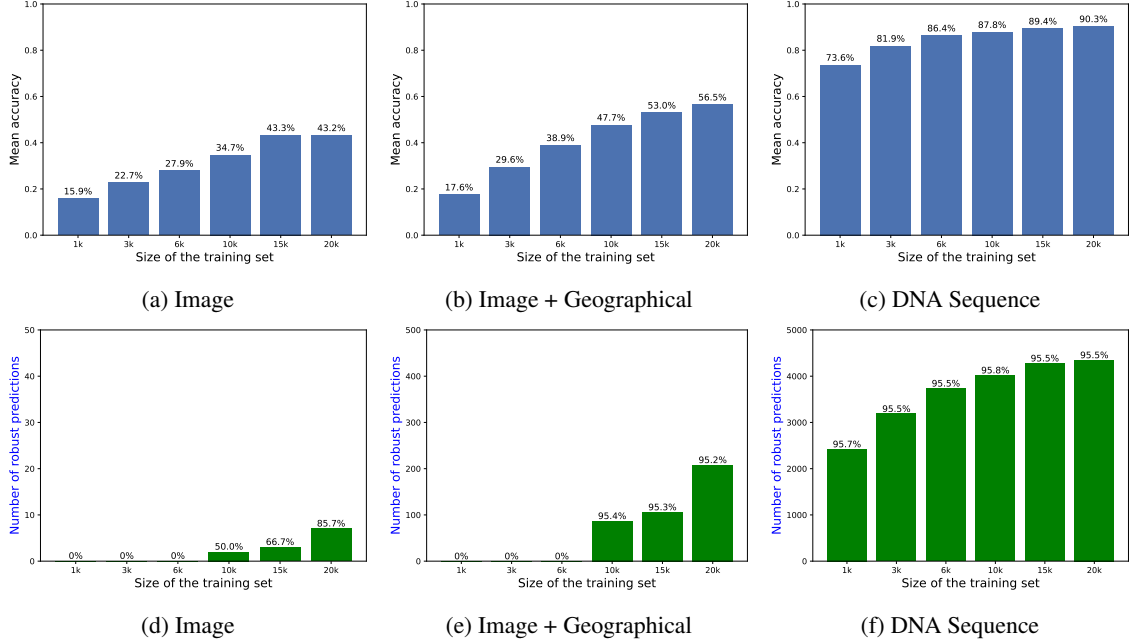


Figure 4: Global test performance (top) and robust predictions with performance on robust predictions (bottom) for each model vs. size of the training set on BIOSCAN-5M dataset with Deep EK-NN.

AU remained high, which hints at the problem remaining too complex. Finally, by collecting the DNA data of the observations, only 3000 instances were needed in the training set to reduce EU. This time, with AU falling below the threshold ($AU \leq t_a$), the decision-making could finally be considered as reliable.

For the second example, the first model can be stopped earlier, requiring only 5000 labeled instances. This time, with the enriched geographical information, AU was deemed sufficiently low. The prediction was therefore considered as reliable, even without the DNA sequence information. In our example, both test instances were correctly classified as *Coleoptera* at the end of the ALFA procedure.

An in-depth study of our experiment, including the method used to determine the thresholds, is provided in Appendix E. Several general insights can be drawn, and are depicted in Figure 4. Naturally, the larger the training set, the better the model’s performance (*i.e.* active learning). Moreover, the number of reliable predictions increases with the number of training observations. This number of reliable predictions also grows with the complexity of the model. For example, the model trained on DNA sequences achieves 90.3% accuracy with 20k training instances. Among the 5000 test instances, 4349 are considered reliable, with a 95.6% accuracy on this subset. In contrast, the model trained on images and enriched with geographical information achieves 56% accuracy with 20k training instances. Among the 5000 test instances, only 208 are considered reliable, yet they achieve a 95.2% accuracy: a significant improvement compared to the 56% overall accuracy. For the first model (trained solely on images), between 0 and 8 predictions are considered reliable with fewer than 20k training instances. However, this number could be drastically increased by adding more observations in the training set (increasing costs), provided the model’s uncertainty is of epistemic nature.

Not only does the proposed method provide a rejection criterion, enabling reliable predictions with a consistent accuracy of approximately 95%, but more importantly, it provides indications so as to why a decision cannot be made and should be rejected instead. If the rejection is epistemic in nature, additional observations need to be collected. If it is aleatoric in nature, acquiring more observations will not be useful, and it becomes necessary to transition to a more complex (and therefore more costly) representation space.

The study was also conducted for other state-of-the-art methods for quantifying uncertainty discussed in the previous experiments. Here too, the ALFA strategy is compatible with all four methods analyzed. However, the centroid-based method faces greater challenges in making reliable predictions on image data and exhibits low accuracy in the DNA sequence classification task. On the other hand, although it does not achieve the best performance on image data, Deep EK-NN significantly outperforms the other methods in generating reliable predictions for DNA sequence classification (as detailed in Appendix E).

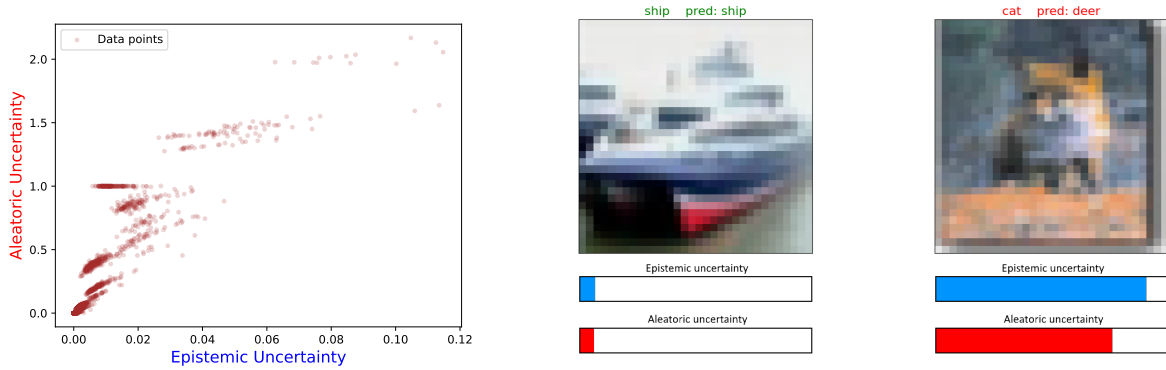


Figure 5: Aleatoric uncertainty vs. Epistemic uncertainty on CIFAR-10 with ResNet18 exhibiting a positive correlation ($\simeq 0.89$). This is a perfectly reasonable phenomenon associated with image datasets and not an issue of disentanglement. Ships are well-represented (low EU) and easy to classify (low AU), whereas cats that resemble deer (or foxes) are rare (high EU) and also difficult to distinguish (high AU).

4.3 Insights on uncertainty disentanglement

The decomposition of AU and EU has recently received criticism (Wimmer et al., 2023; de Jong et al., 2024) and a recent study (Mucsányi et al., 2024) argued that this disentanglement may be impossible to achieve. Nonetheless, the statement in this latter study that “no existing approach provides disentangled uncertainty estimators in practice, because AU and EU are correlated for all estimators” is to our opinion not correct. We argue that this correlation is, in fact, a natural phenomenon.

To our opinion, the aforementioned statement is biased by the fact that a single type of dataset was used in the experiments. The study shows a strong positive correlation between EU and AU, but one should be cautious when extending this to imply a lack of disentanglement. This could be due to the data (notably in the case of image datasets, as used in the study). We stress out that rare images (for which knowledge is scarce and therefore EU high), such as a cat that looks like a deer, are also hard to classify (lying at the boundary between two classes, with high AU). Such a correlation may therefore be inherently tied to the dataset.

We replicated the experiment on an image dataset (CIFAR-10 (Krizhevsky, 2009)) using a deep ResNet18 (He et al., 2016) model and Deep EK-NN for uncertainty quantification (see Appendix B); the result is displayed in Figure 5. We also found a positive correlation ($\simeq 0.89$), although somewhat weaker than most of those found in (Mucsányi et al., 2024) on ImageNet (Deng et al., 2009), highlighting similar results. However, we repeated this on other classical datasets from the UCI (Dua & Graff, 2017) repository; the results are also reported in Appendix B. These latter clearly show that the correlation between EU and AU highly depends on the dataset, with some datasets (like Parkinson or Ecoli) not demonstrating any correlation at all.

Caution is therefore required when asserting a lack of disentanglement, where what could be observed in such an experiment might simply be that, in such a dataset, rare observations are also difficult to classify.

5 Conclusion

In conclusion, this paper introduces an active learning strategy that integrates multi-modal feature acquisition to enhance the robustness of machine learning predictions. By employing a reject criterion grounded in the assessment of both epistemic and aleatoric uncertainties, the proposed approach not only delivers robust predictions but also provides a systematic protocol to address uncertainties when predictions lack confidence. This dual-directional sampling strategy (focusing on acquiring additional observations for epistemic uncertainty and new modalities for aleatoric uncertainty) ensures a flexible and cost-effective framework for improving model performance.

The experimental evaluation across two datasets, including a multimodal dataset combining images, geographical data, and DNA sequences, demonstrates the effectiveness of the strategy. By leveraging various state-of-the-art uncertainty quantification methods (whether entropy-based, variance-based, or density-based) the framework showcases its adaptability in mitigating uncertainties while accounting for the associated costs. This work highlights the potential of multi-modal data acquisition in active learning as a robust and resource-efficient paradigm for uncertainty-aware machine learning.

References

- Acosta, J. N., Falcone, G. J., Rajpurkar, P., and Topol, E. J. Multimodal biomedical ai. *Nature Medicine*, 28(9), 1773–1784, 2022.
- Baltrusaitis, T., Ahuja, C., and Morency, L. P. Multimodal machine learning: A survey and taxonomy. *IEEE transactions on Pattern Analysis and Machine Intelligence*, 41(2):423–443, 2018.
- Bengs, V., Hüllermeier, E., and Waegeman, W. Pitfalls of epistemic uncertainty quantification through loss minimisation. In Koyejo, S., Mohamed, S., Agarwal, A., Belgrave, D., Cho, K., and Oh, A. (eds.), *Advances in Neural Information Processing Systems*, volume 35, pp. 29205–29216. Curran Associates, Inc., 2022.
- Bengs, V., Hüllermeier, E., and Waegeman, W. On second-order scoring rules for epistemic uncertainty quantification. In *Proceedings of the 40th International Conference on Machine Learning, ICML’23*. JMLR.org, 2023.
- Charpentier, B., Zügner, D., and Günnemann, S. Posterior network: Uncertainty estimation without ood samples via density-based pseudo-counts. In Larochelle, H., Ranzato, M., Hadsell, R., Balcan, M., and Lin, H. (eds.), *Advances in Neural Information Processing Systems*, volume 33, pp. 1356–1367. Curran Associates, Inc., 2020.
- Charpentier, B., Borchert, O., Zugner, D., Geisler, S., and Günnemann, S. Natural posterior network: Deep Bayesian predictive uncertainty for exponential family distributions. In *ICLR*, 2022.
- Clertant, M., Sokolovska, N., Chevaleyre, Y., and Hanczar, B. Interpretable cascade classifiers with abstention. In Chaudhuri, K. and Sugiyama, M. (eds.), *Proceedings of the Twenty-Second International Conference on Artificial Intelligence and Statistics*, volume 89 of *Proceedings of Machine Learning Research*, pp. 2312–2320. PMLR, 16–18 Apr 2019.
- de Jong, I. P., Sburlea, A. I., and Valdenegro-Toro, M. How disentangled are your classification uncertainties?, 2024. URL <https://arxiv.org/abs/2408.12175>.
- Dempster, A. P. Upper and Lower Probabilities Induced by a Multivalued Mapping. *The Annals of Mathematical Statistics*, 38(2):325 – 339, 1967.
- Deng, J., Dong, W., Socher, R., Li, L.-J., Li, K., and Fei-Fei, L. Imagenet: A large-scale hierarchical image database. In *2009 IEEE Conference on Computer Vision and Pattern Recognition*, pp. 248–255, 2009.
- Deng, Y. Uncertainty measure in evidence theory. *Science China Information Sciences*, 63, 11 2020.
- Denœux, T. A k-nearest neighbor classification rule based on dempster-shafer theory. *Systems, Man and Cybernetics, IEEE Transactions on*, 219, 1995.
- Denœux, T. A neural network classifier based on dempster-shafer theory. *IEEE Transactions on Systems, Man, and Cybernetics - Part A: Systems and Humans*, 30(2):131–150, 2000.
- Depeweg, S., Hernandez-Lobato, J., Doshi-Velez, F., and Udluft, S. Decomposition of uncertainty in Bayesian deep learning for efficient and risk-sensitive learning. In *Proc. ICML, 35th Int. Conf. on Machine Learning*, 2018.
- Douze, M., Guzhva, A., Deng, C., Johnson, J., Szilvasy, G., Mazaré, P.-E., Lomeli, M., Hosseini, L., and Jégou, H. The faiss library, 2024. URL <https://arxiv.org/abs/2401.08281>.
- Dua, D. and Graff, C. UCI ML Repository, 2017. URL <https://archive.ics.uci.edu/>.
- Duan, R., Caffo, B., Bai, H., I Sair, H., and Jones, C. Evidential uncertainty quantification: A variance-based perspective. In *In Proceedings of the IEEE/CVF Winter Conference on Applications of Computer Vision*, 2024.
- Dubois, D. and Prade, H. Properties of measures of information in evidence and possibility theories. *Fuzzy sets and systems*, 24(2):161–182, 1987.
- Dubois, D. and Prade, H. Representation and combination of uncertainty with belief functions and possibility measures. *Computational Intelligence*, 4(3):244–264, 1988.
- Fellaji, M. and Pennerath, F. The epistemic uncertainty hole: an issue of bayesian neural networks, 2024. URL <https://arxiv.org/abs/2407.01985>.
- Gal, Y. *Uncertainty in Deep Learning*. PhD thesis, University of Cambridge, 2016.

- Gharaee, Z., Lowe, S. C., Gong, Z., Arias, P. M., Pellegrino, N., Wang, A. T., Haurum, J. B., Zarubiieva, I., Kari, L., Steinke, D., Taylor, G. W., Fieguth, P., and Chang, A. X. BIOSCAN-5M: A multimodal dataset for insect biodiversity, 2024.
- Greiner, R., Grove, A. J., and Roth, D. Learning cost-sensitive active classifiers. *Artificial Intelligence*, 139(2): 137–174, 2002.
- Hacohen, G., Dekel, A., and Weinshall, D. Active learning on a budget: Opposite strategies suit high and low budgets. In Chaudhuri, K., Jegelka, S., Song, L., Szepesvári, C., Niu, G., and Sabato, S. (eds.), *International Conference on Machine Learning, 2022, Baltimore, Maryland, USA*, volume 162 of *Proceedings of Machine Learning Research*, pp. 8175–8195. PMLR, 2022.
- He, K., Zhang, X., Ren, S., and Sun, J. Deep residual learning for image recognition. In *2016 IEEE Conference on Computer Vision and Pattern Recognition (CVPR)*, pp. 770–778, 2016.
- Hoarau, A., Martin, A., Dubois, J.-C., and Le Gall, Y. Imperfect labels with belief functions for active learning. In *Belief Functions: Theory and Applications*. Springer International Publishing, 2022.
- Hoarau, A., Lemaire, V., Gall, Y., Dubois, J.-C., and Martin, A. Evidential uncertainty sampling strategies for active learning. *Machine Learning*, 113:1–22, 06 2024.
- Hora, S. C. Aleatory and epistemic uncertainty in probability elicitation with an example from hazardous waste management. *Reliability Engineering & System Safety*, 54(2):217–223, 1996. Treatment of Aleatory and Epistemic Uncertainty.
- Houlsby, N., Huszár, F., Ghahramani, Z., and Lengyel, M. Bayesian active learning for classification and preference learning, 2011. URL <https://arxiv.org/abs/1112.5745>.
- Huang, L., Ruan, S., Xing, Y., and Feng, M. A review of uncertainty quantification in medical image analysis: Probabilistic and non-probabilistic methods. *Medical Image Analysis*, 97:103223, 2024.
- Hüllermeier, E. and Waegeman, W. Aleatoric and epistemic uncertainty in machine learning: An introduction to concepts and methods. *Machine Learning*, 110:457–506, 2021.
- Jürgens, M., Meinert, N., Bengs, V., Hüllermeier, E., and Waegeman, W. Is epistemic uncertainty faithfully represented by evidential deep learning methods? In *Proceedings of the 41st International Conference on Machine Learning, ICML’24*. JMLR.org, 2024.
- Kendall, A. and Gal, Y. What uncertainties do we need in bayesian deep learning for computer vision? In *NIPS*, 2017.
- Klir, G. J. and Ramer, A. Uncertainty in the dempster-shafer theory: a critical re-examination. *International Journal of General System*, 18(2):155–166, 1990.
- Klir, G. J. and Wierman, M. J. Uncertainty-based information: Elements of generalized information theory. In *Springer-Verlag*, 1998.
- Kossen, J., Cangea, C., Vértes, E., Jaegle, A., Patraucean, V., Ktena, I., Tomasev, N., and Belgrave, D. Active acquisition for multimodal temporal data: A challenging decision-making task, 2023.
- Krizhevsky, A. Learning multiple layers of features from tiny images. In *University of Toronto*, 2009. URL <https://api.semanticscholar.org/CorpusID:18268744>.
- Lakshminarayanan, B. Practical tutorial on uncertainty and out-of-distribution robustness in deep learning, google research, link: <https://www.gatsby.ucl.ac.uk/balaji/balaji-odsc-talk.pdf>, 2024.
- Lakshminarayanan, B., Pritzel, A., and Blundell, C. Simple and scalable predictive uncertainty estimation using deep ensembles. In *Advances in Neural Information Processing Systems 30: Annual Conference on Neural Information Processing Systems*, pp. 6402–6413, 2017.
- Lefevre, E., Colot, O., and Vannoorenberghe, P. Belief function combination and conflict management. *Information Fusion*, 3(2):149–162, June 2002.
- Lewis, D. D. and Gale, W. A. A sequential algorithm for training text classifiers. In *SIGIR*, 1994.

- Li, Y. and Oliva, J. B. Active feature acquisition with generative surrogate models. In *International Conference on Machine Learning*, 2020.
- Liang, P., Zadeh, A., and Morency, L.-P. Foundations and trends in multimodal machine learning: Principles, challenges, and open questions. *ACM Computing. Surveys*, 2024.
- Liu, W., Wang, X., Owens, J. D., and Li, Y. Energy-based out-of-distribution detection. In *Advances in Neural Information Processing Systems*, volume 2020-December, 2020.
- Malinin, A. and Gales, M. Predictive uncertainty estimation via prior networks. In *Advances in Neural Information Processing Systems 31: Annual Conference on Neural Information Processing Systems*, 2018.
- Malinin, A. and Gales, M. Reverse kl-divergence training of prior networks: Improved uncertainty and adversarial robustness. In *Advances in Neural Information Processing Systems 32: Annual Conference on Neural Information Processing Systems 2019*, 2019.
- Meinert, N., Gawlikowski, J., and Lavin, A. The unreasonable effectiveness of deep evidential regression. In *AAAI Conference on Artificial Intelligence*, 2022.
- Mobiny, A., Yuan, P., Moulik, S., Garg, N., Wu, C., and Nguyen, H. Dropconnect is effective in modeling uncertainty of bayesian deep networks. *Scientific Reports*, 11, 03 2021.
- Mucsányi, B., Kirchhof, M., and Oh, S. J. Benchmarking uncertainty disentanglement: Specialized uncertainties for specialized tasks. In *The Thirty-eight Conference on Neural Information Processing Systems Datasets and Benchmarks Track*, 2024.
- Nguyen, V.-L., Shaker, M. H., and Hüllermeier, E. How to measure uncertainty in uncertainty sampling for active learning. *Machine Learning*, 111:89–122, jan 2022.
- Nguyen, V.-L., Zhang, H., and Destercke, S. Learning sets of probabilities through ensemble methods. In *European Conference on Symbolic and Quantitative Approaches with Uncertainty*, pp. 270–283. Springer, 2023.
- Pedregosa, F., Varoquaux, G., Gramfort, A., Michel, V., Thirion, B., Grisel, O., Blondel, M., Prettenhofer, P., Weiss, R., Dubourg, V., Vanderplas, J., Passos, A., Cournapeau, D., Brucher, M., Perrot, M., and Duchesnay, E. Scikit-learn: Machine learning in Python. *Journal of Machine Learning Research*, 12:2825–2830, 2011.
- Quost, B. Decision-making from partial instances by active feature querying. In Cano, A., De Bock, J., Miranda, E., and Moral, S. (eds.), *Proceedings of the Twelfth International Symposium on Imprecise Probability: Theories and Applications*, volume 147 of *Proceedings of Machine Learning Research*, pp. 264–272. PMLR, 06–09 Jul 2021.
- Sale, Y., Hofman, P., Wimmer, L., E., H., and Nagler, T. Second-order uncertainty quantification: Variance-based measures., 2023.
- Sale, Y., Hofman, P., Löhr, T., Wimmer, L., Nagler, T., and Hüllermeier, E. Label-wise aleatoric and epistemic uncertainty quantification, 2024. URL <https://arxiv.org/abs/2406.02354>.
- Schweighofer, K., Aichberger, L., Lelanskyi, M., and Hochreiter, S. Introducing an improved information-theoretic measure of predictive uncertainty. In *In NeurIPS 2023 Workshop on Mathematics of Modern Machine Learning*, 2023.
- Sensoy, M., Kaplan, L., and Kandemir, M. Evidential deep learning to quantify classification uncertainty. In Bengio, S., Wallach, H., Larochelle, H., Grauman, K., Cesa-Bianchi, N., and Garnett, R. (eds.), *Advances in Neural Information Processing Systems*, volume 31. Curran Associates, Inc., 2018.
- Settles, B. Active learning literature survey. Computer Sciences Technical Report 1648, University of Wisconsin–Madison, 2009.
- Shafer, G. *A Mathematical Theory of Evidence*. Princeton University Press, 1976.
- Shaker, M. H. and Hüllermeier, E. Aleatoric and epistemic uncertainty with random forests. In Berthold, M. R., Feelders, A., and Kreml, G. (eds.), *Advances in Intelligent Data Analysis XVIII*, pp. 444–456, Cham, 2020. Springer International Publishing.
- Shannon, C. E. A mathematical theory of communication. *Bell System Technical Journal*, 27(3):379–423, 1948.

- Shelmanov, A., Puzyrev, D., Kupriyanova, L., Belyakov, D., Larionov, D., Khromov, N., Kozlova, O., Artemova, E., Dylov, D. V., and Panchenko, A. Active learning for sequence tagging with deep pre-trained models and Bayesian uncertainty estimates. In Merlo, P., Tiedemann, J., and Tsarfaty, R. (eds.), *Proceedings of the 16th Conference of the European Chapter of the Association for Computational Linguistics: Main Volume*, pp. 1698–1712, Online, April 2021. Association for Computational Linguistics.
- Shim, H., Hwang, S. J., and Yang, E. Joint active feature acquisition and classification with variable-size set encoding. In Bengio, S., Wallach, H., Larochelle, H., Grauman, K., Cesa-Bianchi, N., and Garnett, R. (eds.), *Advances in Neural Information Processing Systems*, volume 31. Curran Associates, Inc., 2018.
- Smets, P. and Kennes, R. The transferable belief model. *Artificial Intelligence*, 1994.
- Sun, Y., Ming, Y., Zhu, X., and Li, Y. Out-of-distribution detection with deep nearest neighbors, 2022. URL <https://arxiv.org/abs/2204.06507>.
- Tong, Z., Xu, P., and Denœux, T. An evidential classifier based on dempster-shafer theory and deep learning. *Neuro-computing*, 450:275–293, 08 2021.
- Ulmer, D., Hardmeier, C., and Frellsen, J. Prior and posterior networks: A survey on evidential deep learning methods for uncertainty estimation. *Transactions of Machine Learning Research*, 2023.
- Van Amersfoort, J., Smith, L., Teh, Y. W., and Gal, Y. Uncertainty estimation using a single deep deterministic neural network. In III, H. D. and Singh, A. (eds.), *Proceedings of the 37th International Conference on Machine Learning*, volume 119 of *Proceedings of Machine Learning Research*, pp. 9690–9700. PMLR, 13–18 Jul 2020.
- Wimmer, L., Sale, Y., Hofman, P., Bischl, B., and Hüllermeier, E. Quantifying aleatoric and epistemic uncertainty in machine learning: Are conditional entropy and mutual information appropriate measures? In Evans, R. J. and Shpitser, I. (eds.), *Proceedings of the Thirty-Ninth Conference on Uncertainty in Artificial Intelligence*, volume 216 of *Proceedings of Machine Learning Research*, pp. 2282–2292. PMLR, 31 Jul–04 Aug 2023.
- Yager, R. R. On the dempster-shafer framework and new combination rules. *Information Sciences*, 41(2):93–137, 1987.
- Zheng, Z. and Padmanabhan, B. On active learning for data acquisition. In *2002 IEEE International Conference on Data Mining, 2002. Proceedings.*, pp. 562–569, 2002.

A Uncertainty estimation with Deep EK-NN

One of the proposed methods for quantifying uncertainty used in this paper is introduced here. This section presents the framework for representing uncertainty, the tools used to quantify both epistemic and aleatoric uncertainty within this framework, and the application of this model to a machine learning scenario.

A.1 Uncertainty representation

In this framework, we represent uncertainty in the form of belief functions. The theory of belief functions, also known as Dempster-Shafer theory (Dempster, 1967; Shafer, 1976) provides an alternative to probability theory.

The frame of discernment, denoted by Ω , is the set of C exclusive hypotheses such that $\Omega = \{\omega_1, \dots, \omega_C\}$. The power set of the frame, denoted by 2^Ω , represents the set of all subsets of Ω . A source s can then assign a belief to any element of 2^Ω .

The function $m : 2^\Omega \rightarrow [0, 1]$, which assigns belief (or mass) to each element of 2^Ω , is called the mass function and always satisfies the following normalization condition:

$$\sum_{A \in 2^\Omega} m(A) = 1. \quad (8)$$

Non-zero mass elements are called focal elements, and the union of focal elements forms the core. When multiple sources express themselves, it is possible to combine two or more mass functions defined on the same frame of discernment. Several methods exist, each with its own advantages and disadvantages depending on the fusion context (*cf.* (Yager, 1987; Dubois & Prade, 1988; Lefevre et al., 2002)). The conjunctive combination (Dempster’s rule) of two mass functions m_1 and m_2 , defined on the same frame of discernment Ω , is denoted by $m_1 \oplus m_2$ and is defined as follows: for all $A \subseteq \Omega$,

$$m_1 \oplus m_2(A) = \frac{1}{1 - \kappa} \sum_{B \cap C = A} m_1(B)m_2(C), \quad (9)$$

where κ is the degree of conflict defined as:

$$\kappa = \sum_{B \cap C = \emptyset} m_1(B)m_2(C), \quad (10)$$

where B and C are subsets of Ω . This rule is commutative and associative, making it straightforward to extend to combinations of more than two sources.

It is possible and sometimes necessary to make a decision on the frame of discernment Ω , in which case a common strategy is to transform the initial belief function into a probability. One of those transformations results in the pignistic probability distribution *BetP* (Smets & Kennes, 1994):

$$BetP(\{\omega\}) = \sum_{A \in 2^\Omega, \omega \in A} \frac{m(A)}{|A|}. \quad (11)$$

The pignistic probability $BetP(\omega)$ is exactly the Shapley value derived from the mass function.

Example A.1. Assume a murder has been committed and three suspects are considered: Alice, Bob, and Eve, forming the frame of discernment $\Omega = \{\text{Alice}, \text{Bob}, \text{Eve}\}$. During a trial, two reliable sources, s_1 and s_2 , express the following beliefs: “the culprit’s name has three letters”, represented by the mass function $m_1 : m_1(\{\text{Bob}, \text{Eve}\}) = 1$, and “the culprit is a woman” represented by the mass function $m_2 : m_2(\{\text{Alice}, \text{Eve}\}) = 1$. These two pieces of evidence can be combined into m such that $m = m_1 \oplus m_2$, resulting in $m(\{\text{Eve}\}) = 1$, meaning “the culprit is Eve”.

A.2 Uncertainty quantification

Within the evidential framework, multiple quantification measures can be used (Deng, 2020) to represent different kinds of uncertainty. The Hartley entropy measure was extended to the evidential framework (Dubois & Prade, 1987) and Non-specificity has been advocated (Klir & Wierman, 1998) as the best measure of the evidential framework for capturing EU. The Non-specificity NS of a mass function m is defined as:

$$NS(m) = \sum_{A \subseteq \Omega} m(A) \log_2(|A|) \quad (12)$$

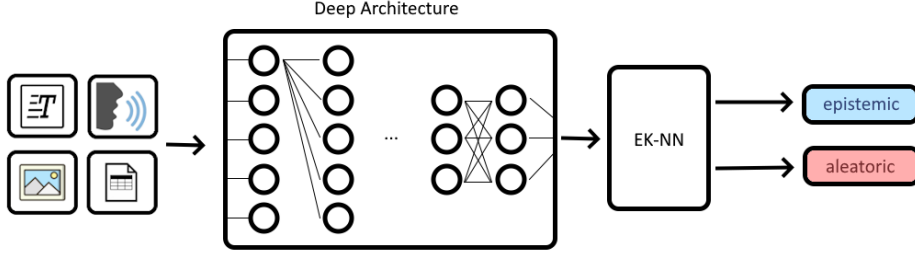


Figure 6: The proposed Deep EK-NN framework used to quantify epistemic and aleatoric uncertainties.

with $|A|$ the cardinality of the set A .

To quantify AU, we use Discord (Klir & Ramer, 1990). It represents the amount of conflicting information, considered of an aleatoric nature. The discord D of a mass function m is defined as:

$$D(m) = - \sum_{A \subseteq \Omega} m(A) \log_2(\text{Bet}P(A)), \quad (13)$$

with $\text{Bet}P(A)$ the pignistic probability of the belief function associated with the event A . As its form suggests, it is an extension of Shannon entropy (Shannon, 1948) to the evidential framework.

Example A.2. Consider the toss of a coin that may or not be fair. The two events h : “the coin lands on heads” and t : “the coin lands on tails” form a partition of the frame $\Omega = \{h, t\}$. Two sources s_1 and s_2 express their beliefs about this coin. Source s_1 states “I don’t know whether the coin is biased or not” with $m_1 : m_1(\{h\}) = 0, m_1(\{t\}) = 0, m_1(\{h, t\}) = 1$, while source s_2 expresses “I know that the coin is not biased” with $m_2 : m_2(\{h\}) = 0.5, m_2(\{t\}) = 0.5, m_2(\{h, t\}) = 0$. The Non-specificity in m_1 is $NS(m_1) = 1$. This represents maximal EU, as s_1 is in a state of complete ignorance. The Non-specificity in m_2 is $NS(m_2) = 0$, meaning the EU is zero, and the Discord in m_2 is $D(m_2) = 1$, meaning the AU is maximal, since m_2 corresponds to a purely aleatoric event, of a fair coin toss.

A.3 Estimating epistemic and aleatoric uncertainties with Deep EK-NN

In this paper, we introduce our Deep EK-NN framework, available at: <https://github.com/ArthurHoa/deep-eknn>. This framework enables the quantification of epistemic and aleatoric uncertainties for most deep learning architectures. Notably, the framework is compatible with pre-trained models and can be seamlessly placed at the penultimate layer of a neural network (whether convolutional, residual, transformer, encoder, *etc.*) to perform uncertainty quantification and separation, as illustrated in Figure 6. It relies on EK-NN (Evidential K-Nearest Neighbors) (Denœux, 1995) to predict the membership of a new incoming observation in the form of a belief function. Essentially, the nearest neighbors of the instance to be classified are treated as sources of information, which are combined using Dempster’s rule of combination (at Equation (9), see example A.1). The class membership of each neighbor is discounted based on its distance from the instance being predicted, with greater ignorance assigned when closest neighbors are further away. EK-NN has been extended to neural networks in (Denœux, 2000) and more recently to deep convolutional networks in (Tong et al., 2021). In deep learning, a similar approach from a different body of literature has been employed for out-of-distribution detection (Sun et al., 2022).

With the proposed framework, we provide a straightforward method for quantifying uncertainty that is compatible with most deep architectures. Observations are encoded using the penultimate layer of a neural network, and EK-NN is then applied to this reduced feature space, producing a belief function as output. EU and AU are subsequently computed according to Equations (13) and (12), respectively.

Inspired by (Sun et al., 2022), we slightly modified the implementation by incorporating fast neighbor search (Douze et al., 2024) and an approximate mean distance calculation for the γ parameter to handle large datasets efficiently. However, this new framework is no longer inherently compatible with missing labels, partial labels, or rich labels, as the classical EK-NN was.

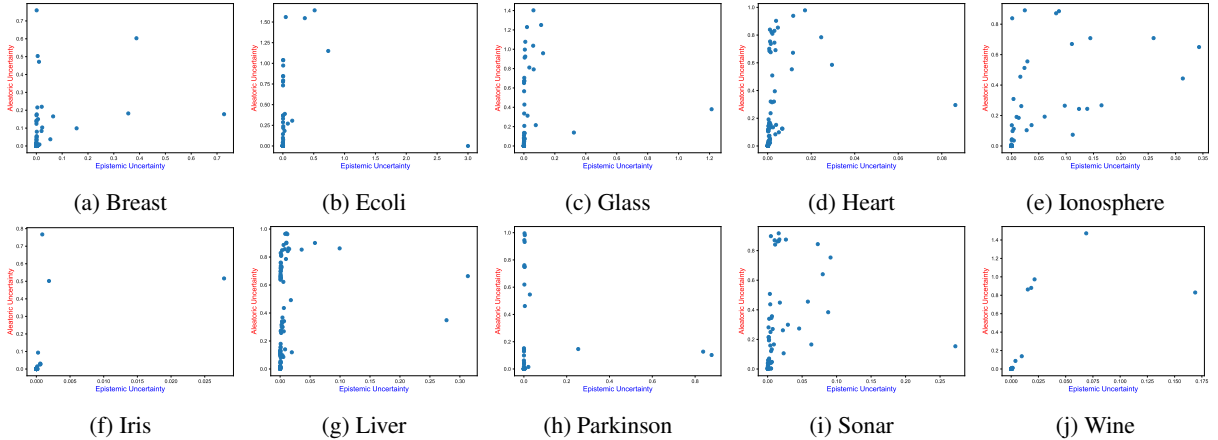


Figure 7: Epistemic uncertainty vs. Aleatoric uncertainty.

Table 1: Pearson correlation vs. Dataset, exhibiting a varying correlation.

DATASET	CORR	P-VALUE	SIGNIFICANCE
BREAST CANCER	0.36	$1.1 * 10^{-6}$	✓
ECOLI	0.14	$1.6 * 10^{-1}$	×
GLASS	0.12	$3.3 * 10^{-6}$	×
HEART	0.27	$9.0 * 10^{-3}$	✓
IONOSPHERE	0.61	$3.1 * 10^{-12}$	✓
IRIS	0.52	$2.0 * 10^{-4}$	✓
LIVER	0.17	$8.0 * 10^{-2}$	×
PARKINSON	-0.02	$9.0 * 10^{-1}$	×
SONAR	0.22	$7.8 * 10^{-2}$	×
WINE	0.66	$5.1 * 10^{-8}$	✓

B Uncertainty disentanglement

For this experiment, the disentanglement between epistemic and aleatoric uncertainties is studied across multiple datasets. CIFAR-10 (Krizhevsky, 2009) is a 10-class dataset consisting of 32x32 colored images, divided into 50k images for the training set and 10k images for the test set. Some additional UCI datasets (Dua & Graff, 2017) are also used for further discussion. For these datasets, we randomly split the training and test sets with a 70/30 ratio.

For classical machine learning datasets, the EK-NN model (Denceux, 1995) was used to estimate epistemic and aleatoric uncertainties. The parameters are the same as those used in the γ -EKNN version presented by (Hoarau et al., 2022). For this experiment, we arbitrarily chose a number K of neighbors equal to 7. The model functions as a classical K-nearest neighbors model, treating the neighbors as sources of information. The class of each neighbor is transformed into a belief function (e.g. an observation labeled “cat” sees its label converted to $m(\{\text{cat}\}) = 1$), and this mass is discounted toward ignorance $m(\Omega)$, based on the distance to the observation being predicted (e.g. it may become $m(\{\text{cat}\}) = 0.1, m(\Omega) = 0.9$ if the neighbor is very distant). For the γ parameter, which defines the discounting applied based on the distance of the neighbors, we used the average distance between all points in the training set.

All neighbors masses are then combined into the predicted belief function using Equation (9), therefore Non-specificity (12) and Discord (13) can be directly computed as epistemic and aleatoric uncertainties, respectively. Epistemic and aleatoric uncertainties for these 10 datasets are depicted in Figure 7, highlighting little to no correlation or a debatable relationship. Such as in (Mucsanyi et al., 2024), Pearson correlations are computed and p-values for a risk $\alpha = 0.05$ are depicted in Table 1 along the correlation coefficient.

For the CIFAR-10 dataset, a ResNet18 (He et al., 2016) is pre-trained on the dataset (see the work of <https://github.com/kuangliu/pytorch-cifar> for a Python implementation). The proposed Deep EK-NN framework can then be directly applied after this step to estimate epistemic and aleatoric uncertainties. A single pass through

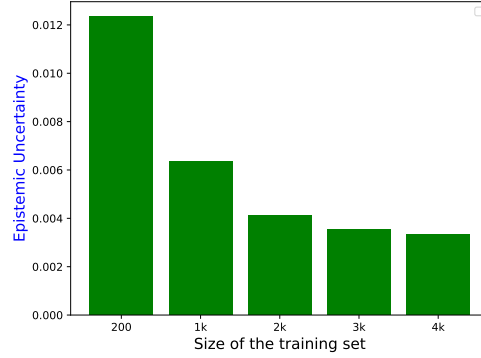


Figure 8: Monotonicity of the epistemic uncertainty for the proposed model on different sizes of CIFAR-10 with ResNet18.

the network is first performed up to its penultimate layer to extract a reduced 512-variable feature space for both the training and test sets. From this point, an analogous EK-NN training process can be carried out with an arbitrary $K = 10$ neighbors.

C Monotonicity of epistemic uncertainty

Another point of discussion in the literature is the quality of the model’s EU estimation. Some authors (Bengs et al., 2022) have formalized axioms that a second-order probability should satisfy to achieve a proper estimation of epistemic uncertainty. Among these axioms is the monotonicity of EU with respect to the addition of information, a natural property that any learner should indeed adhere to. Plainly put, the model should become progressively less ignorant as it acquires more information, a crucial property for our proposed strategy.

However, as was recently shown (Jürgens et al., 2024; Bengs et al., 2023; Meinert et al., 2022), second-order risk minimization cannot guarantee compliance with such properties. Furthermore, it was experimentally demonstrated (Jürgens et al., 2024) that EU is not necessarily decreasing and is strongly dependent on the regularization term for this family of methods. Similar concerns have been raised regarding Bayesian deep learning (Fellaji & Pennerath, 2024).

Nevertheless, Deep EK-NN satisfies this axiom. The Non-specificity measure (Dubois & Prade, 1987) used here allows for EU to decrease as information is combined. This is illustrated in Figure 8, which displays EU estimates for models trained on the CIFAR-10 dataset with increasing training set size. The observed behavior aligns with expectations: EU decreases while the models become progressively less ignorant as more information is added.

D Application to Wine dataset

The dataset (Dua & Graff, 2017) consists of wines grown in the same region of Italy but derived from three different cultivars. Each sample is characterized by 13 variables, which we have grouped based on an assigned fictitious cost, defined as follows:

Ignition study Ash, Alcalinity of ash, Total phenols, Non-flavenoid phenols

Visual study Hue, Color intensity

Chemical study Proanthocyanins, Flavanoids, Magnesium, od315 of diluted wines

Acidity study Proline, Malic acid, Alcohol

For the experiments, we randomly split the training and test sets using a 70/30 ratio, run the experiments, and repeat the process 100 times to estimate the mean performance.

Four different models are trained on the dataset according to the train/test split. The first model is trained solely on the variables from the ignition study. The second model is trained on the same variables enriched with those from the visual study, and so on, until the fourth model incorporates all 13 variables.

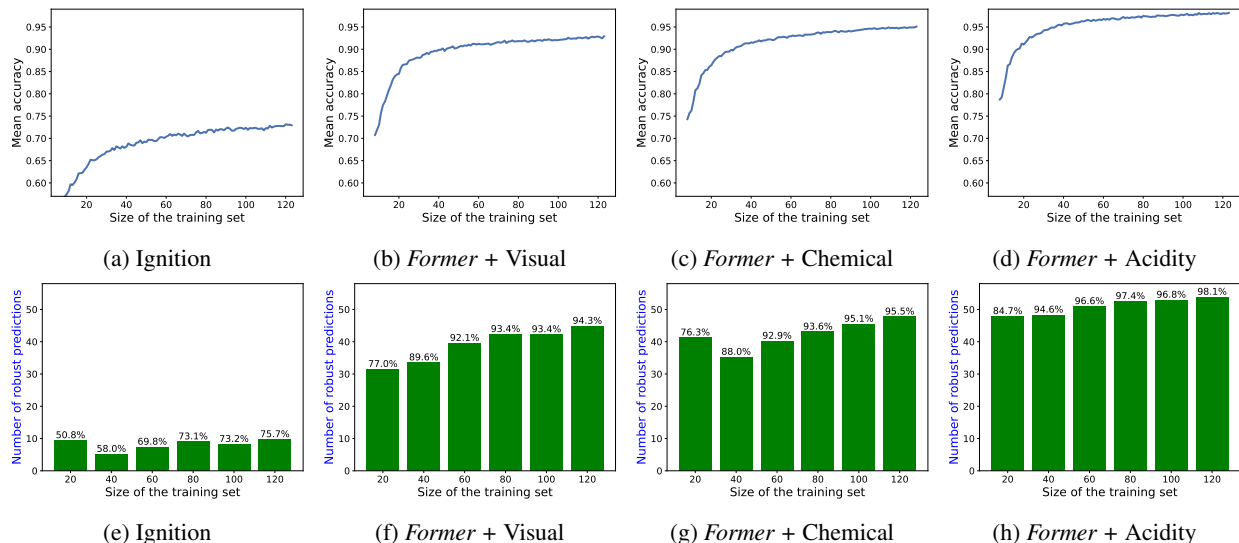


Figure 9: Entropy based uncertainty estimation: global test performance (top) and robust predictions with performance on robust predictions (bottom) for each model vs. size of the training set on Wine dataset.

For the first model, accuracy, epistemic uncertainty, and aleatoric uncertainty are computed using the proposed Deep EK-NN framework. We used the same parameters as in the previous section and arbitrarily set the number of neighbors K to 7. The second, third, and fourth models are trained in the same way using their respective variable spaces.

The performance of each model, based on the number of training instances, is presented in Figure 3. Figure 3a illustrates the performance improvement of the model trained on the four ignition study variables as the training set increases from 8 to 124 observations. The accuracy on the entire test set ranges from 55% to 75%. The results in the following figures demonstrate the expected behavior: a more complex representation space yields better performance for any given training set size. However, the difference in performance is less pronounced between the second and third models, indicating that the newly added variables are not particularly informative.

In the second row, Figures 3e to 3h show the number of robust predictions according to ALFA as a function of the number of training instances. A prediction is considered robust if both epistemic and aleatoric uncertainties are below their respective thresholds. In all figures, the accuracy on the subset of robust predictions is also shown and is consistently higher than the accuracy on the full test set, which is the expected behavior for a reject criterion.

D.1 Entropy based ensemble method

The experiment is also conducted using the entropy-based ensemble method presented in (Shaker & Hüllermeier, 2020) to estimate epistemic and aleatoric uncertainties.

For the dataset, the same protocol as in the previous experiment is followed. The proposed method is replaced by a random forest with 100 estimators and a maximum depth of 4. All other parameters are set to the default values of the scikit-learn library (Pedregosa et al., 2011).

To compute epistemic and aleatoric uncertainties, we used the entropy decomposition proposed in (Shaker & Hüllermeier, 2020), where the total uncertainty is defined as the entropy of the posterior distribution and epistemic uncertainty is measured as the mutual information. Their paper describes an approximation of these measures to avoid integration over the hypothesis space.

Similar to the first experiment, the performance of each of the four models, based on the number of training instances, is presented in the first row of Figure 9. In the second row, each figure shows the number of robust predictions according to ALFA as a function of the number of training instances.

D.2 Variance based ensemble method

Another experiment with the same protocol is additionally performed with the variance-based ensemble method described in (Sale et al., 2024) to assess epistemic and aleatoric uncertainties.

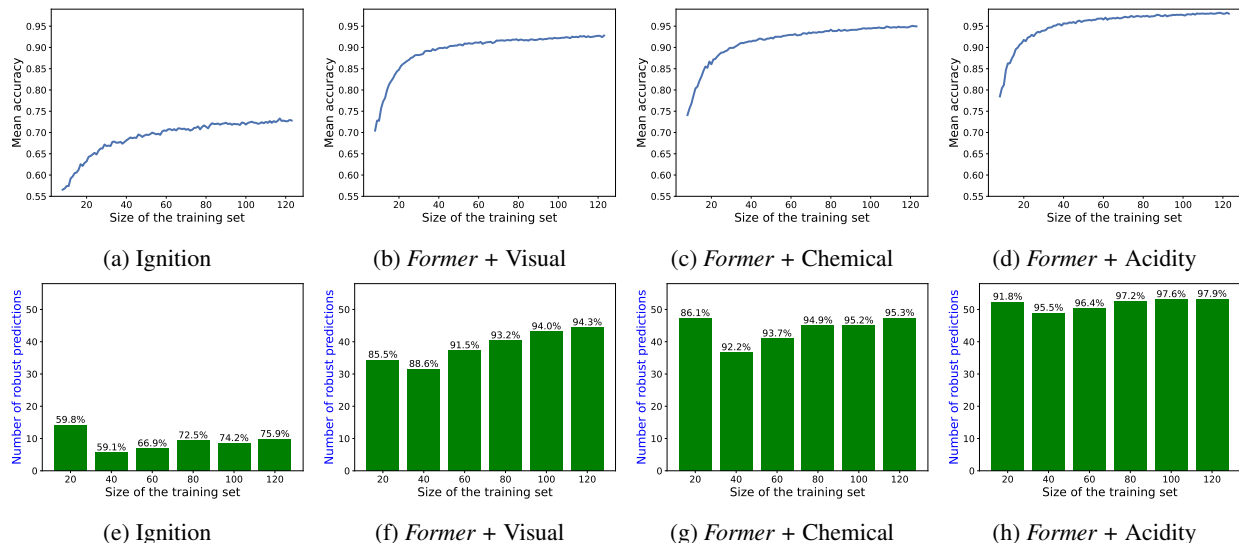


Figure 10: Variance based uncertainty estimation: global test performance (top) and robust predictions with performance on robust predictions (bottom) for each model vs. size of the training set on Wine dataset.

The model is also replaced by a random forest with 100 estimators and a maximum depth of 4 (identical to the previous one). All other parameters are set to the default values of the scikit-learn library (Pedregosa et al., 2011).

To compute epistemic and aleatoric uncertainties, we employed the label-wise variance decomposition proposed in (Sale et al., 2024). In this approach, total uncertainty for each class is defined as the variance of the outcome, and the global uncertainty is obtained by summing over all classes. Aleatoric uncertainty is defined as the expected conditional variance, while epistemic uncertainty corresponds to the expected reduction in squared-error loss. Their paper also provides a direct Python implementation of the proposed equations.

Similar to the other experiments, the performance of each of the four models, based on the number of training instances, is presented in the first row of Figure 10. In the second row, each figure shows the number of robust predictions according to ALFA as a function of the number of training instances.

D.3 Centroid based density method

Finally, the centroid-based approach presented in (Van Amersfoort et al., 2020) is also examined. To compute the model’s uncertainty, the authors propose measuring the distance from the incoming observation to the nearest class centroid using a radial basis function. Since they do not provide an aleatoric/epistemic decomposition, we propose using their measure as an epistemic uncertainty metric. This is justified because it relies on density and is, therefore, dependent on the epistemic state of the learner. To compute aleatoric uncertainty, we normalized the proposed distances to all centroids by their sum, creating a probability mass function. Classical Shannon entropy is then calculated to determine the aleatoric uncertainty.

Centroids are computed for each class in the training set using Euclidean distance (a neural network is not employed in this experiment, so the weight matrix is ignored). The predicted class is determined by maximizing the criterion proposed by the authors, which is a certainty measure rather than an uncertainty measure. The inverse of this value is taken as the epistemic uncertainty, and the aleatoric uncertainty is obtained as described earlier. The length scale parameter is set to $\sqrt{0.1}$.

As in the other experiments, the performance of each of the four models, based on the number of training instances, is shown in the first row of Figure 11. In the second row, each figure depicts the number of robust predictions, according to ALFA, as a function of the number of training instances.

D.4 Overview of the results

All four explored methods performed as expected with more variance for low numbers of robust predictions (statistical limit). An overview of the results are presented in Table 2 and Table 3.

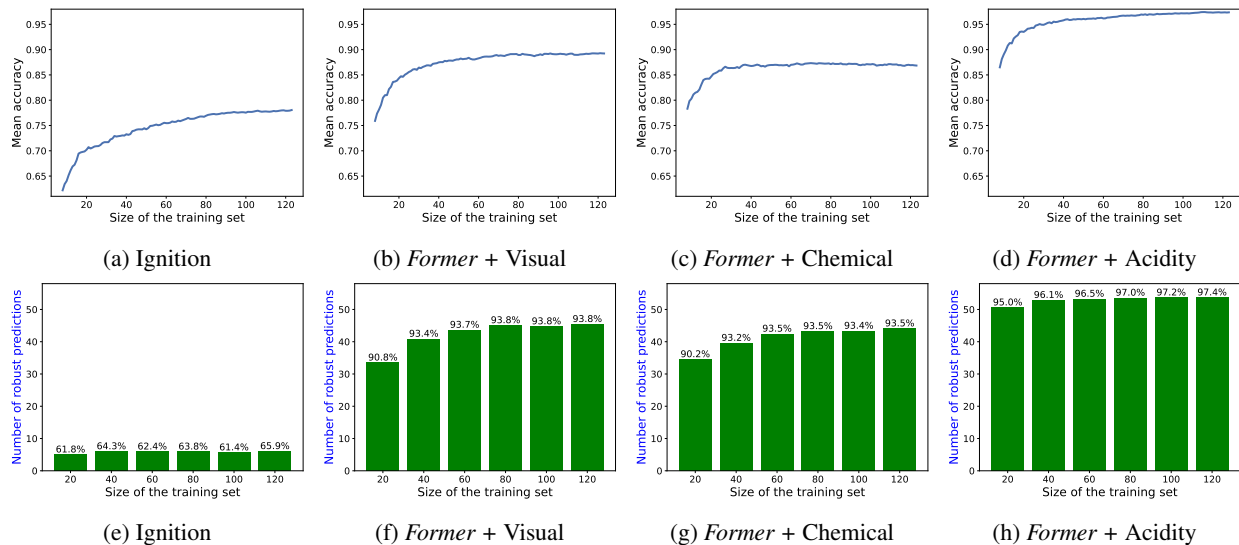


Figure 11: Centroid based uncertainty estimation: global test performance (top) and robust predictions with performance on robust predictions (bottom) for each model vs. size of the training set on Wine dataset.

Method	Ignition	+ Visual	+ Chemical	+ Acidity	Method	Ignition	+ Visual	+ Chemical	+ Acidity
Entropy-based	8	39	42	51	Entropy-based	66.8%	90.0%	90.2%	95.0%
Variance-based	9	39	44	52	Variance-based	68.1%	91.2%	92.9%	96.1%
Centroid-based	6	42	42	53	Centroid-based	63.2%	93.2%	93.0%	96.5%
Deep EK-NN	13	41	43	52	Deep EK-NN	80.7%	93.2%	93.5%	95.9%

Table 2: Mean number of robust predictions vs. model complexity for each of the four studied methods on Wine dataset.

Table 3: Mean accuracy of robust predictions vs. model complexity for each of the four studied methods on Wine dataset.

Table 2 presents the mean number of robust predictions for each model according to ALFA, as well as for the four studied methods for quantifying uncertainty. Table 3 shows the mean performance of the studied methods on the subset of the test set considered robust.

The ALFA procedure is compatible with all four studied methods. It is worth noting that density-based methods (centroids and Deep EK-NN) slightly outperform ensemble-based methods in terms of robust predictions and overall performance. However, in our view, more important than performance is compliance with the expected behavior. Density-based methods demonstrate smoother monotonicity in the plotted curves, reflecting a more consistent quantification of uncertainty.

E Application to BIOSCAN-5M

The BIOSCAN-5M (Gharaee et al., 2024) dataset is a multi modal dataset for insect biodiversity. Pictures of insects are collected along with geographical information and DNA sequences are collected. For our experiment we used a subset of BIOSCAN-5M of $50k$ training instances and $5k$ test instances uniformly distributed over 10 classes (biological orders of the class *Insecta*), they are presented in Figure 12.

Three different models are trained on the dataset according to the train/test split. The first model is trained solely on the images, the second model is trained on both the images and the geographical information, and the third model is trained solely on the DNA sequences. For the images, we used a ResNet18 model. The images were resized to a $64 \times 64 \times 3$ tensor, and normalization was applied based on ImageNet statistics. We employed a cross-entropy loss with stochastic gradient descent (SGD), using a learning rate of 0.1^1 , momentum of 0.9, and a weight decay of 5×10^{-4} . Each batch had a size of 100, and the models were trained for 10 epochs.

¹The learning rate for each parameter group was also set using a cosine annealing schedule.

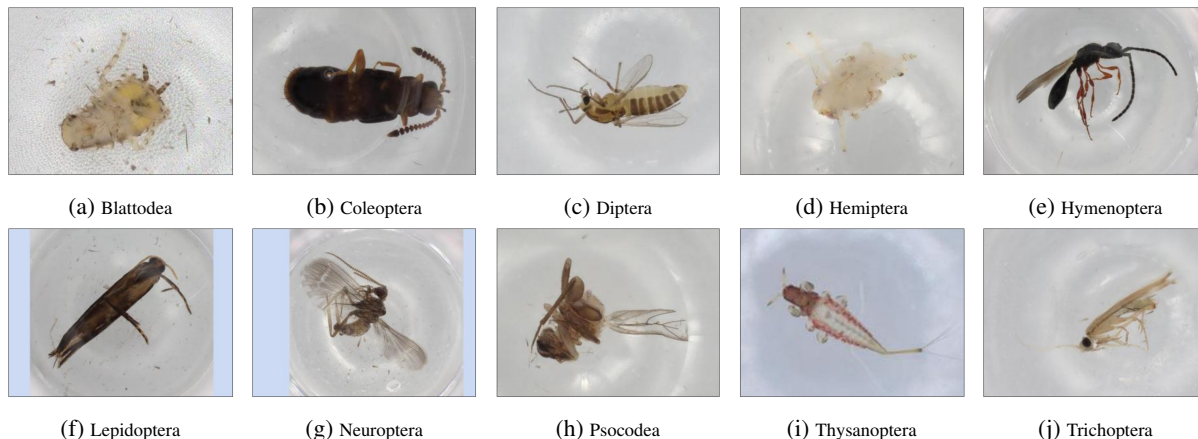


Figure 12: BIOSCAN-5M: 10 orders for the class *Insecta*.

For the first model, after training, the epistemic and aleatoric uncertainties can be computed by applying the proposed Deep EK-NN framework to the penultimate layer of the ResNet18. We used the same parameters as presented in the previous section and arbitrarily set the number of neighbors K to 10.

For the second model, after training, a reduced feature space is extracted from the ultimate layer of the ResNet18. This feature space is then enriched with the geographical information: country and state are encoded using one-hot encoding, while latitude and longitude are included as numerical values. Both sets of features are standardized. Finally, the same Deep EK-NN framework is applied to compute the epistemic and aleatoric uncertainties.

For the third model, only DNA sequences are considered. We used k -mer frequency feature extraction with $k = 3$ to encode the DNA sequences. From this feature space, the Deep EK-NN framework can also be applied to compute epistemic and aleatoric uncertainties. Note that, in this case, it is seamlessly integrated into a more classical machine learning scenario.

The performance of each model based on the number of training instances is presented in Figure 4. Figure 4a illustrates the performance improvement of the image model as the training set increases from $1k$ to $20k$ observations. The accuracy on the entire test set ranges from 15.9% to 43.3%. Figures 4a, 4b, and 4c demonstrate the expected behavior: a more complex representation space, although more expensive to collect, yields better performance for any given training set size.

On the second line, Figures 4d, 4b, and 4c show the number of robust predictions as a function of the number of training instances. A prediction is considered robust if both epistemic and aleatoric uncertainties are below their respective thresholds. The next section explains how these thresholds were selected. In all figures, the accuracy on the reduced subset of robust predictions is also shown and is consistently higher than the accuracy on the full test set, which is the expected behavior of a reject criterion.

Figure 4d shows that for the first model, the predictions are not confident enough to be considered robust, with a maximum of only 7 robust predictions out of 5000. This number can be increased by either relaxing the thresholds or adding more observations in the training set. However, the latter approach will only be effective if the model's uncertainty is primarily epistemic in nature. The observed trend of an increasing number of robust predictions, along with the fact that deep learning models for images typically require more than few thousands of examples, suggests that collecting more labels can indeed lead to more robust predictions. This can be directly addressed with the proposed method, which quantifies the remaining epistemic and aleatoric uncertainties.

Figure 4e shows a significant increase in the number of robust predictions once the training set includes $10k$ observations, reaching more than 200 robust predictions at $20k$. For both models shown in Figures 4e and 4f, where a substantial number of robust predictions are achieved, the accuracy of these robust predictions consistently exceeds 95%. This means that each robust prediction has more than a 95% chance of being correct, which is a considerable improvement compared to the 47.7% accuracy at $10k$ for the second model.

Figure 4f demonstrates that with a well-performing model, it is possible to achieve a significant number of robust predictions, more than 4200 out of 5000, given the defined thresholds. The proposed method ensures that such expensive models are only used when it is not possible to obtain a robust prediction using a less costly approach.

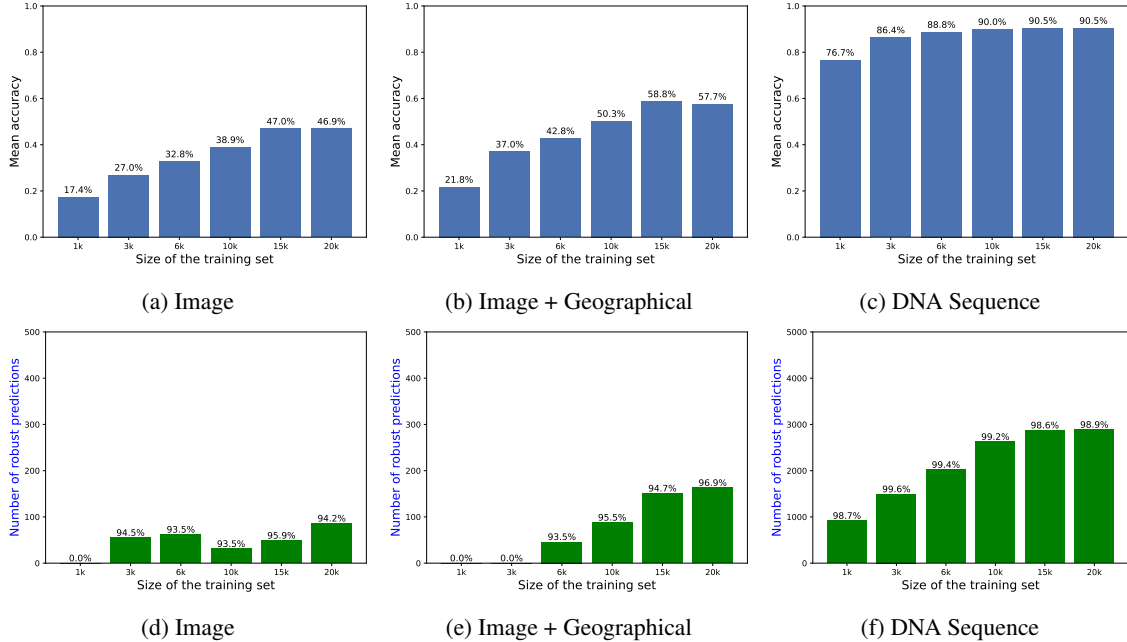


Figure 13: Entropy based uncertainty estimation: global test performance (top) and robust predictions with performance on robust predictions (bottom) for each model vs. size of the training set on BIOSCAN-5M dataset.

E.1 Entropy-based ensemble method

To enable a fair comparison, we used the same deep learning model trained exclusively on the images. Specifically, we employed the ResNet18 model to reduce the variable space. The images were resized to a $64 \times 64 \times 3$ tensor, and normalization was applied using ImageNet statistics. A cross-entropy loss function was used alongside stochastic gradient descent (SGD) with a learning rate of 0.1, momentum of 0.9, and a weight decay of 5×10^{-4} . Each batch consisted of 100 samples, and the models were trained for 10 epochs.

For the first model, after training, epistemic and aleatoric uncertainties were computed in the representation space obtained from the penultimate layer of ResNet18. The same method described in the Wine section was applied. A Random Forest model, trained with 100 estimators and a minimum of 10 samples per leaf, was used. All other parameters were set to the default values provided by the scikit-learn library (Pedregosa et al., 2011).

For the second model, after training, a reduced feature space was extracted from the final layer of ResNet18. This feature space was then enriched with geographical information: country and state were encoded using one-hot encoding, while latitude and longitude were included as numerical values. Both sets of features were standardized. The same entropy-based framework was subsequently applied to compute epistemic and aleatoric uncertainties.

For the third model, only DNA sequences were considered. k -mer frequency feature extraction with $k = 3$ was used to encode the DNA sequences. This feature space was then analyzed using a Random Forest model with 100 estimators and a maximum depth of 10.

Epistemic and aleatoric uncertainties for all three models were computed as described in the Wine experiment. Similar to the first method, the performance of the three models, based on the number of training instances, is illustrated in the first row of Figure 13. The second row of figures shows the number of robust predictions, as defined by ALFA, as a function of the number of training instances.

E.2 Variance-based ensemble method

The same setup as the previous method is repeated for the variance-based uncertainty estimation. We employed the same ResNet18 model to reduce the variable space. The images were resized to a $64 \times 64 \times 3$ tensor, and normalization was applied using ImageNet statistics. A cross-entropy loss function was used alongside stochastic gradient descent (SGD) with a learning rate of 0.1, momentum of 0.9, and a weight decay of 5×10^{-4} . Each batch consisted of 100 samples, and the models were trained for 10 epochs.

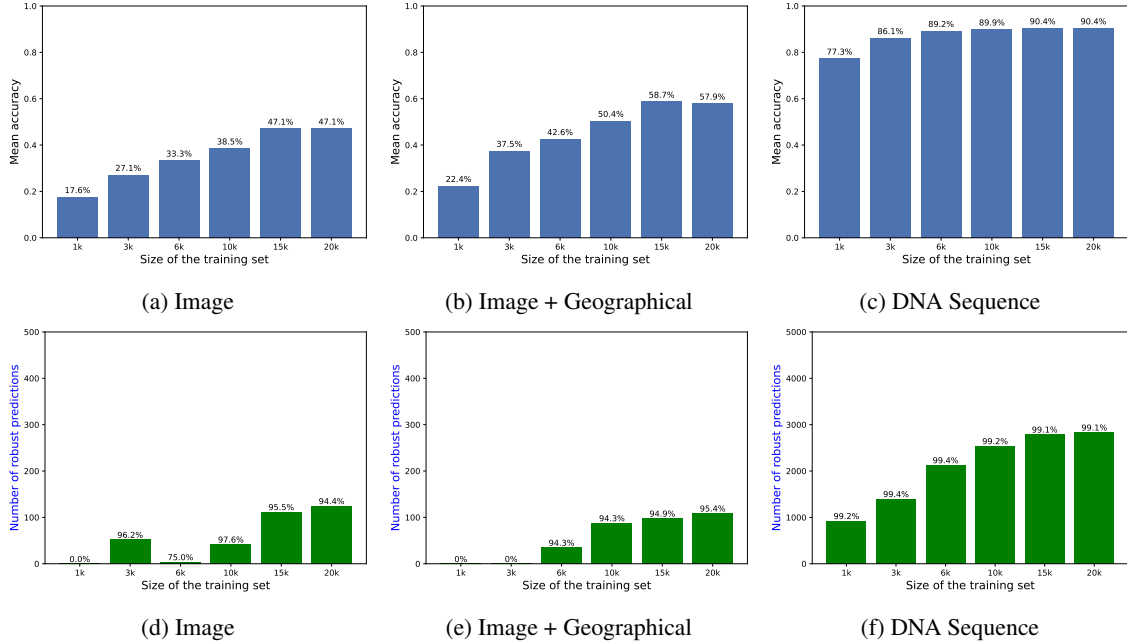


Figure 14: Variance based uncertainty estimation: global test performance (top) and robust predictions with performance on robust predictions (bottom) for each model vs. size of the training set on BIOSCAN-5M dataset.

For the first model, after training, epistemic and aleatoric uncertainties were computed in the representation space obtained from the penultimate layer of ResNet18. The same method described in the Wine section was applied. A Random Forest model, trained with 100 estimators and a minimum of 8 samples per leaf, was used. All other parameters were set to the default values provided by the scikit-learn library (Pedregosa et al., 2011).

For the second model, after training, a reduced feature space was extracted from the final layer of ResNet18. This feature space was then enriched with geographical information: country and state were encoded using one-hot encoding, while latitude and longitude were included as numerical values. Both sets of features were standardized. The same variance-based framework was subsequently applied to compute epistemic and aleatoric uncertainties.

For the third model, only DNA sequences were considered. k -mer frequency feature extraction with $k = 3$ was used to encode the DNA sequences. This feature space was then analyzed using a Random Forest model with 100 estimators and a maximum depth of 8.

Epistemic and aleatoric uncertainties for all three models were computed as described in the Wine experiment. Similar to the first and second methods, the performance of the three models, based on the number of training instances, is illustrated in the first row of Figure 14. The second row of figures shows the number of robust predictions, as defined by ALFA, as a function of the number of training instances.

E.3 Centroid-based density method

This final method differs slightly from the previous three, as centroids must be updated during every batch in a deep learning scenario. Consequently, the implementation is somewhat different. However, to ensure a fair comparison, a similar ResNet18 (He et al., 2016) architecture is trained using common parameters and the same number of epochs. The authors of the method (Van Amersfoort et al., 2020) provide a PyTorch implementation of their approach, which we used for training the model.

The images were resized to a $64 \times 64 \times 3$ tensor, and normalization was applied using ImageNet statistics. A cross-entropy loss function was used alongside stochastic gradient descent (SGD) with a learning rate of 0.05, momentum of 0.9, and a weight decay of 5×10^{-4} . Each batch consisted of 100 samples, and the models were trained for 10 epochs. This methods require the last layer of the ResNet to be modified (from 10 outputs to 512). In each batch, the centroids are updated according to the proposed method described by the authors, and the uncertainties can be calculated in the same manner as in the Wine experiment.

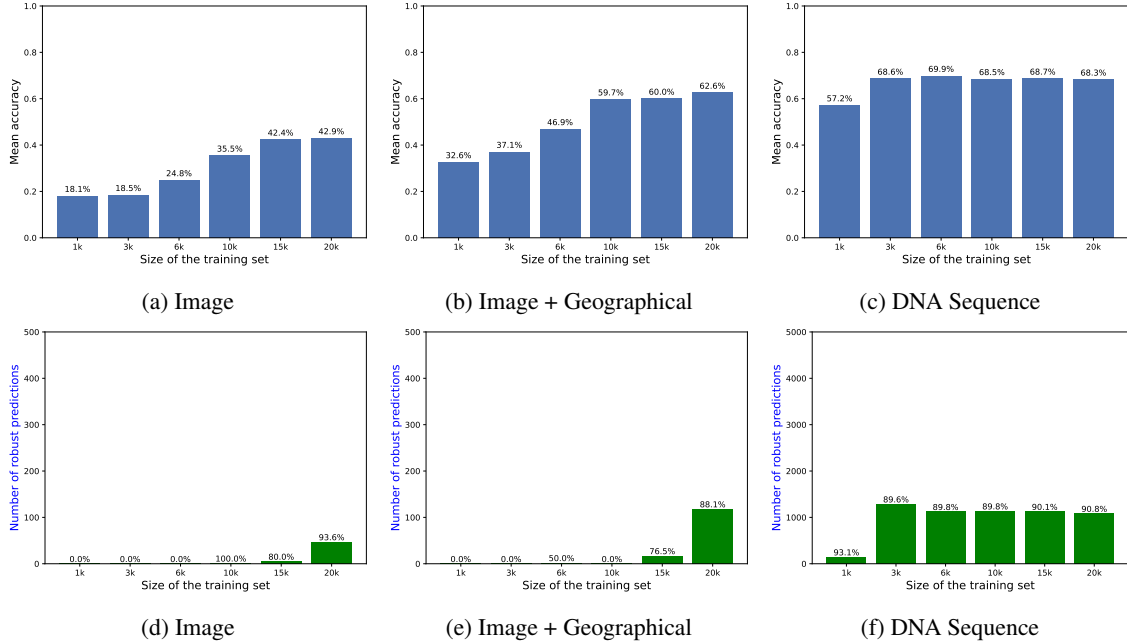


Figure 15: Centroid based uncertainty estimation: global test performance (top) and robust predictions with performance on robust predictions (bottom) for each model vs. size of the training set on BIOSCAN-5M dataset.

For the first model, after training, epistemic and aleatoric uncertainties were computed in the representation space obtained from the final layer of the ResNet18. The same method described in the Wine section was applied, with a length scale of 0.1.

For the second model, after training, a reduced feature space was extracted from the final layer of the ResNet18. This feature space was then enriched with geographical information: country and state were encoded using one-hot encoding, while latitude and longitude were included as numerical values. Both sets of features were standardized. The same centroid-based framework was subsequently applied to compute epistemic and aleatoric uncertainties, with a length scale of $\sqrt{0.1}$.

For the third model, which was not trained using a deep architecture, only DNA sequences were considered. The DNA sequences were encoded using k -mer frequency feature extraction with $k = 3$. The same method described in the Wine experiments was then applied to this reduced feature space, using a length scale of $\sqrt{0.1}$.

Similar to the first and second methods, the performance of the three models, based on the number of training instances, is illustrated in the first row of Figure 15. The second row of figures shows the number of robust predictions, as defined by ALFA, as a function of the number of training instances.

E.4 Overview of the results

Both entropy-based and variance-based ensemble methods, as well as the proposed Deep EK-NN framework, performed as expected with respect to ALFA. The centroid-based density method also performed coherently but this kind of approach seem less effective on classification of DNA sequences. An overview of the results are presented in Table 4 and Table 5.

Table 4 presents the mean number of robust predictions for each model according to ALFA, as well as for the four studied methods for quantifying uncertainty. Table 3 shows the mean performance of the studied methods on the subset of the test set considered robust.

The ALFA procedure is compatible with all four methods studied. However, the centroid-based method struggles to make robust predictions when using the high selected risk threshold of $\alpha = 0.05$ (*c.f.*, next Section). This method also performs worse in DNA sequence classification, as a centroid-based approach is not particularly efficient in such a task compared to other methods, such as a simple K-NN strategy with k -mer frequency feature extraction.

Method	Image	Image + Geographical	DNA
Entropy-based	47	75	2137
Variance-based	56	55	2101
Centroid-based	9	23	983
Deep EK-NN	2	67	3669

Table 4: Mean number of robust predictions vs. model complexity for each of the four studied methods on BIOSCAN.

Method	Image	Image + Geographical	DNA
Entropy-based	94.3%	95.1%	99.1%
Variance-based	91.7%	94.7%	99.3%
Centroid-based	91.2%	71.5%	90.5%
Deep EK-NN	67.5%	95.3%	96.0%

Table 5: Mean accuracy of robust predictions vs. model complexity for each of the four studied methods on BIOSCAN.

F Thresholds selection

Many approaches could be considered to determine suitable thresholds. Here, we propose allowing experts to select the thresholds based on the specific application. To facilitate this, we introduce a parameter $\alpha \in [0, 1]$, which accounts for the desired level of risk associated with each threshold.

To determine the thresholds, an unseen validation set is set aside, and the epistemic and aleatoric uncertainties of the model are computed for each instance. These uncertainty values are then ranked in descending order, and observations are sequentially rejected until the accuracy of the remaining observations reaches $(1 - \alpha) * 100$. This procedure is performed separately for epistemic uncertainties to obtain the epistemic threshold t_e , and for aleatoric uncertainties to determine the aleatoric threshold t_a . It is important to note that, in practical applications or method comparisons, the test set cannot be used to compute these thresholds. The test set should only be used once for final evaluation (following the “vault assumption”, where opening the test set renders it no longer valid for unbiased evaluation).

In all our experiments, we used a risk $\alpha = 0.05$, which can explain the 95% accuracy achieved by robust predictions in Figures 4e and 4f.